

Surface Reaction and Topography Modeling of Fluorocarbon Plasma Etching

Frâncio Rodrigues*, Luiz Felipe Aginsky*, Alexander Toifl*, Alexander Scharinger*, Andreas Hössinger†, and Josef Weinbub*

*Christian Doppler Laboratory for High Performance TCAD,

Institute for Microelectronics, TU Wien, Gußhausstraße 27-29, 1040 Wien, Austria

†Silvaco Europe Ltd., Compass Point, St Ives, Cambridge, PE27 5JL, United Kingdom

Email: rodrigues@iue.tuwien.ac.at

Abstract—Fluorocarbon plasma etching is a key enabling technology for modern semiconductor fabrication processes. Particularly, fluorocarbon etching of SiO₂ via structures finds a wide variety of applications in logic and memory devices. The etching technology’s development is, however, hindered by the complexity of the surface phenomena and by the intricacy of the etchant flux distribution on the feature scale. We thus propose a revised surface reaction model for fluorocarbon plasma etching processes to study these effects. The surface model is integrated into a TCAD workflow and is applied to a via etch process of SiO₂ by C₄F₈/O₂/Ar. The model is calibrated with experimental data and is able to accurately reproduce the via shape, overall etch rate (560 nm/min), and mask faceting angle (60°). We then apply the workflow to investigate essential process information that would otherwise require substantial experimental effort. The etch rate dependence with time throughout the 90 s process is analyzed and correlated with the aspect ratio dependent etching lag effect. We find that for aspect ratios > 7 the etch rate falls below 500 nm/min, which causes a substantial increase in total etch time for deeper vias.

I. INTRODUCTION

The continuous advancements of semiconductor device performance and down-scaling demands ever-growing progress in fabrication technologies. Among the key challenging fabrication steps is plasma etching, in particular, when considering ever-denser structures with increasingly demanding high aspect ratios (HARs) [1]. Due to the complexity of plasma etching, long trial and error procedures are commonplace during the development of new fabrication workflows. Accurate and efficient modeling of dry etching is thus essential to aid manufacturing developments by providing a virtual process prototyping tool

which in addition to accurate process modeling allows to improve the understanding of plasma etching technologies.

Feature scale modeling of dry etching is an important tool to investigate surface phenomena and the etch rate topography dependency. Fluorocarbon plasma-related surface phenomena are particularly hard to predict due to the simultaneous etching and deposition reactions. However, it is precisely this complex interplay that enables the fabrication of HAR structures [1], underlining the importance of accurately modeling these joint reactions. Visibility effects regarding the distribution of reactants add to that complexity and give rise to undesirable effects such as aspect ratio dependent etching (ARDE) [2]. Surface reactions and topography dependencies have been investigated in previous studies [3]–[5].

In this work, we contribute to these efforts by proposing a revised surface reaction model, describing SiO₂ plasma etching by C₄F₈/O₂/Ar. The model has been integrated into a representative process technology computer-aided design (TCAD) workflow. We calibrate the model based on experimental data, characterize the etch rate evolution over time, its dependency on the via aspect ratio, and discuss mask faceting.

II. TCAD WORKFLOW

We implemented the here proposed revised surface reaction model into Silvaco’s *Victory Process* [6] and use the simulator’s ray tracing [7], [8] and level-set engines [9] for visibility calculations and the topography evolution, respectively (Fig. 1). The ray tracer is used to calculate the flux of reactants taking into account different source distributions and visibility effects. The flux calculations serve as an input to a Langmuir set

of coverage equations (1-3) that describes the surface reaction mechanisms. The polymer coverage (4) determines whether polymer deposition (5) or etching (6) occurs. The level-set engine applies the rates to the surface and updates the geometry accordingly.

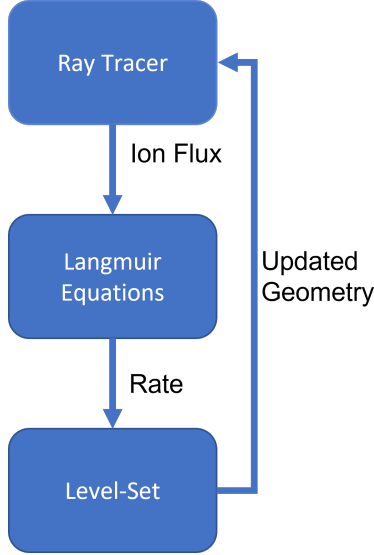


Fig. 1. TCAD Workflow. The ray tracer evaluates the local ion flux following a *von Mises* source distribution. Langmuir equations combine the ion flux with parameters from Table I and calculate the etch or deposition rates. At last, the level-set engine evolves the surface accordingly.

We abstract the intricate plasma composition into three functional particles: neutrals (n), ions (i), and polymers (p). The subscript n/p indicates neutrals on top of a polymer substrate. Neutrals act as etchants, polymers as etching inhibitors as well as the depositing species of a polymer layer, and ions cause sputtering and reactive ion etching (RIE) mechanisms. Neutrals and polymers cover the substrate surface following a Langmuir adsorption model (1-3), where each right-hand side term represents a mechanism of adsorption or etching (RIE, evaporation, sputtering). The main quantities in (1-3) are the coverages $\Theta_{n,p}$ which represent the fraction of substrate surface sites covered by n or p . The polymer can also be etched, therefore, $\Theta_{n/p}$ (3) describes the coverage of polymers by neutrals to take polymer etching into account. Equations (1-3) are solved under a steady-state approximation ($\frac{d\Theta_{n,p,n/p}}{dt} = 0$) because the surface evolves very slowly compared to the time scale of adsorption and desorption mechanisms [3]. The remaining variables present in (1-6) are the fluxes $J_{n,i,p}$, the sticking coefficients $S_{n,p,n/p}$, the stoichiometric coefficient k_n , the substrate densities for polymer (ρ_p) and SiO_2

(ρ_{SiO_2}), the rates R_{dep} and R_{etch} , the sputtering yield Y_s , and the RIE yields $Y_{n,n/p}$. J_{ev} is the evaporation flux and k_{ev} its stoichiometric constant and both are used to model the thermal evaporation etching mechanism [3].

$$\frac{d\Theta_n}{dt} = J_n S_n (1 - \Theta_n - \Theta_p) - J_i Y_n k_n \Theta_n - J_{ev} k_{ev} \Theta_n \quad (1)$$

$$\frac{d\Theta_p}{dt} = J_p S_p - J_i Y_{n/p} \Theta_n \Theta_{n/p} \quad (2)$$

$$\frac{d\Theta_{n/p}}{dt} = J_n S_{n/p} (1 - \Theta_{n/p}) - J_i Y_{n/p} \Theta_{n/p} \quad (3)$$

$$\Theta_p = \frac{J_p S_p}{J_i Y_{n/p} \Theta_{n/p}} \quad (4)$$

$$R_{dep} = \frac{J_i Y_{n/p} - J_p S_p}{\rho_p} \quad (5)$$

$$R_{etch} = \frac{1}{\rho_{\text{SiO}_2}} (J_i Y_i \Theta_n + J_i Y_s (1 - \Theta_n - \Theta_p) + J_{ev} k_{ev} \Theta_n) \quad (6)$$

The yield values $Y_{n,n/p,s}$ are calculated for each surface element as a function of the impinging ion energy (E) and the angle of ion incidence with respect to the surface normal (ϕ) [10]. The energy dependency is identical for RIE and sputtering mechanisms, but they differ with respect to their ϕ dependency. The RIE related yields $Y_{n,n/p}(E, \phi)$ follow a cosine law (7) while the sputtering yield is given by (8) [3]. The values for the yield constants A , B and for all parameters from equations (1-8) are listed in Table I.

$$Y_{n,n/p}(E, \phi) = A_{n,n/p} (\sqrt{E} - \sqrt{E_{th}}) \cos \phi \quad (7)$$

$$Y_s(E, \phi) = A_s (\sqrt{E} - \sqrt{E_{th}}) (1 + B \sin^2 \phi) \cos \phi \quad (8)$$

Θ_p (4) allows to interpret whether a deposition or etching step occurs: If the surface is completely covered by polymers $\Theta_p \geq 1$ and the polymer deposition rate is given by (5). In turn, if $\Theta_p < 1$ the substrate is etched at a rate given by (6). Compared to other work [3], [11], we revised the model by including Θ_p in the sputtering term of (6) – see red term, because we consider that the fraction of the surface covered

by polymers does not contribute to the pure sputtering etch mechanism. With this revision, the sputtering contribution to the total etch rate is therefore modulated only by the exposed part of the surface. This is also coherent with the abstraction that the polymer particles act as etch inhibitor.

III. RESULTS

We compare our simulations to experimental data from [12] to calibrate and validate our model. Table I summarizes the experimental setup. Fig. 2 shows the initial via geometry and the via state after an etch time (t) of 45 s. We consider the experimentally measured fluorine and ion flux as our neutrals and ion flux input. The evaporation flux and the yield functions are calculated with parameters from [3]. Our fitting parameters are the distributions of the angular sources and the polymer flux.

TABLE I
EXPERIMENTAL AND MODELING PARAMETERS

Symbol	Value	Source
J_n	$1.0 \times 10^{17} \text{ cm}^{-2} \text{ s}^{-1}$	[12]
J_i	$6.0 \times 10^{16} \text{ cm}^{-2} \text{ s}^{-1}$	[12]
J_{ev}	$2.0 \times 10^{14} \text{ cm}^{-2} \text{ s}^{-1}$	[3]
k_n, k_{ev}	2	[3]
$S_{n,p,n/p}$	0.1	[12]
E	1450 eV	[12]
E_{th}	4 eV	[13]
E_{th}	18 eV	[13]
A_n	$0.0361 \text{ eV}^{-1/2}$	[13]
$A_{n/p}$	$0.1444 \text{ eV}^{-1/2}$	[13]
A_s	$0.0139 \text{ eV}^{-1/2}$	[13]
B	9.3	[3]
ρ_{SiO_2}	$2.2 \times 10^{22} \text{ cm}^{-3}$	[3]
ρ_p	$2.0 \times 10^{22} \text{ cm}^{-3}$	[3]
t	90 s	[12]

We use a constant flux value for the neutral and polymer particles across the surface and a sharp *von Mises* source distribution for the ions. The neutrals and polymers constant approximation is appropriate for low sticking particles impinging into HAR features [14]. We fit the polymer flux and the ion *von Mises* distribution based on the agreement of our etch values and final via shape with etch rate values and a micrographry from [12]. J_p was fitted to be $1.6 \times 10^{16} \text{ cm}^{-2} \text{ s}^{-1}$ and the *von Mises* shape parameter to 250. Here, J_p represents the excess C-F species that deposit a polymer instead of etching [12]. J_p also captures the effect of O_2 as a scavenger that

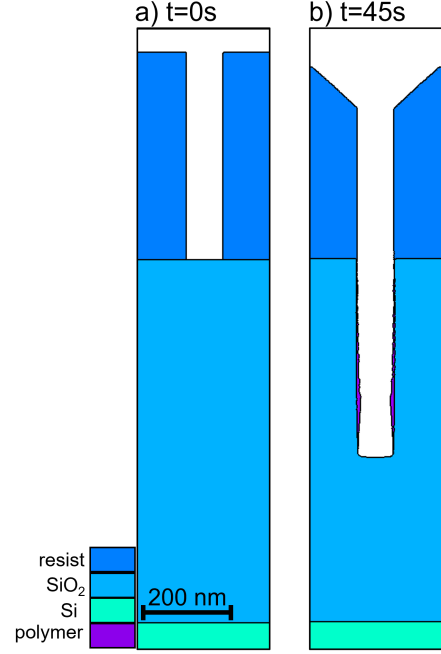


Fig. 2. a) Initial experimental setup with a 85 nm opening and a resist height of 470 nm. b) After 45 s of etch time the resist layer is thinner, exhibits faceting, and the polymer layer at the via sidewalls is evident.

removes excess C-F species to decrease polymer deposition [12].

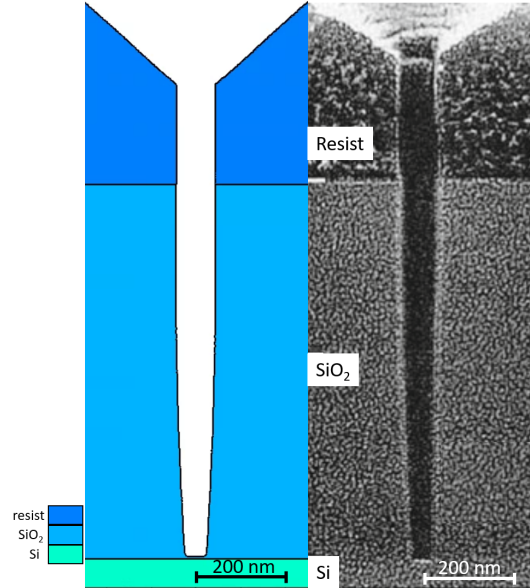


Fig. 3. Comparison of simulated and experimental via after 90 s of etch time. Reprinted with permission from [12], Copyright 1999, American Vacuum Society.

With two fitting parameters, we are able to reproduce the via topography from [12] (Fig. 3). The etch rate for the entire 90 s procedure was 560 nm/min, well inside the measured range of 500 – 600 nm/min. Our mask etch rate of 80 nm/min is also inside the reported range and

its faceting structure closely resembles the experimental via. The faceting structure is a direct consequence of the angular dependency of equation (8) and is expected for materials in which physical sputtering is the main etching mechanism [15]. The simulation faceting angle of 60° is slightly higher than the experimental value of 57° .

Fig. 4 depicts the etch rate evolution with time and via aspect ratio. The ARDE lag for this particular experiment is characterized and shows that the etch rate falls below $500 \text{ nm}/\text{min}$ for aspect ratios > 7 , representing a substantial increase in total etch time for higher aspect ratio feature fabrication.

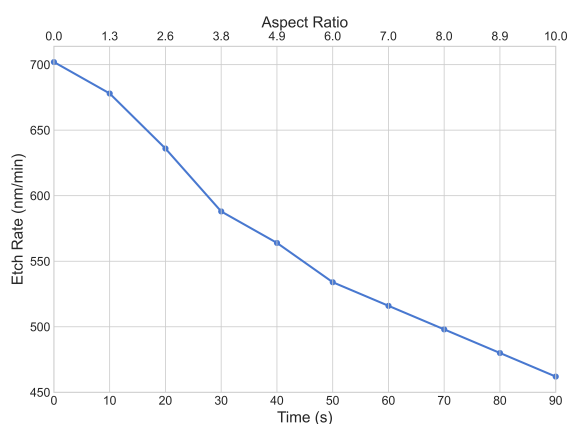


Fig. 4. Etch rate as a function of time and aspect ratio. Our average etch rate of $560 \text{ nm}/\text{min}$ is within the experimental range of $500 - 600 \text{ nm}/\text{min}$ [12] and ARDE lag is reproduced and characterized.

IV. CONCLUSION

We present a revised surface reaction model for fluorocarbon plasma etching and integrate it to a TCAD workflow. The TCAD workflow is applied to a via etch step of SiO_2 by $\text{C}_4\text{F}_8/\text{O}_2/\text{Ar}$. We calibrate the model by comparing the via topography and etch rates to experimental data. The calibrated model is applied to characterize the etch rate evolution over time and its dependency on the via aspect ratio. This workflow can be extended to different materials and plasma etching chemistries, provide input for a device simulator, and is a quick and cost-effective tool to optimize plasma etching processes.

ACKNOWLEDGMENT

The financial support by the Austrian Federal Ministry for Digital and Economic Affairs, the National

Foundation for Research, Technology and Development, and the Christian Doppler Research Association is gratefully acknowledged.

REFERENCES

- [1] T. Iwase, Y. Kamaji, S. Y. Kang *et al.*, “Progress and perspectives in dry processes for nanoscale feature fabrication: Fine pattern transfer and high-aspect-ratio feature formation,” *Japanese Journal of Applied Physics*, vol. 58, no. SE, p. SE0802, Jun 2019.
- [2] C. G. Lee, K. J. Kanarik, and R. A. Gottscho, “The grand challenges of plasma etching: A manufacturing perspective,” *Journal of Physics D: Applied Physics*, vol. 47, no. 27, Jul 2014.
- [3] A. L. Magna and G. Garozzo, “Factors affecting profile evolution in plasma etching of SiO_2 : Modeling and experimental verification,” *Journal of The Electrochemical Society*, vol. 150, no. 10, p. F178, Oct 2003.
- [4] S. Huang, C. Huard, S. Shim, S. K. Nam, I.-C. Song, S. Lu, and M. J. Kushner, “Plasma etching of high aspect ratio features in SiO_2 using $\text{Ar}/\text{C}_4\text{F}_8/\text{O}_2$ mixtures: A computational investigation,” *Journal of Vacuum Science & Technology A*, vol. 37, no. 3, p. 031304, May 2019.
- [5] H. S. You, Y. G. Yook, W. S. Chang *et al.*, “Universal surface reaction model of plasma oxide etching,” *Journal of Physics D: Applied Physics*, vol. 53, no. 38, p. 10, Sep 2020.
- [6] Silvaco, “Silvaco Victory Process,” 2021. [Online]. Available: www.silvaco.com/tcad/victory-process-3d/
- [7] P. Manstetten, J. Weinbub, A. Hössinger, and S. Selberherr, “Using temporary explicit meshes for direct flux calculation on implicit surfaces,” *Procedia Computer Science*, vol. 108, pp. 245–254, Nov 2017.
- [8] A. Scharinger, P. Manstetten, A. Hössinger, and J. Weinbub, “Generative model based adaptive importance sampling for flux calculations in process TCAD,” in *Proc. SISPAD*, 2020, pp. 39–42.
- [9] J. A. Sethian, *Level set methods and fast marching methods: Evolving interfaces in computational geometry, fluid mechanics, computer vision, and materials science*. Cambridge University Press, 1999, vol. 3.
- [10] I. K. Kiyotaka Wasa and H. Kotera, *Handbook of Sputter Deposition Technology*, 2nd ed. Elsevier, 2012.
- [11] X. Klemenschits, S. Selberherr, and L. Filipovic, “Modeling of gate stack patterning for advanced technology nodes: A review,” *Micromachines*, vol. 9, no. 12, p. 631, Nov 2018.
- [12] T. Tatsumi, Y. Hikosaka, S. Morishita, M. Matsui, and M. Sekine, “Etch rate control in a 27 MHz reactive ion etching system for ultralarge scale integrated circuit processing,” *Journal of Vacuum Science & Technology A*, vol. 17, p. 1562, Jul 1999.
- [13] E. Gogolides, P. Vauvert, G. Kokkoris, G. Turban, and A. G. Boudouvis, “Etching of SiO_2 and Si in fluorocarbon plasmas: A detailed surface model accounting for etching and deposition,” *Journal of Applied Physics*, vol. 88, no. 10, pp. 5570–5584, Nov 2000.
- [14] A. Yanguas-Gil, *Growth and Transport in Nanostructured Materials*. Springer, 2017.
- [15] A. G. Nagy, “Sidewall tapering in reactive ion etching,” *Journal of The Electrochemical Society*, vol. 132, no. 3, pp. 689–693, Mar 1985.